

This PDF has been sent from one of the University of Delaware's partner libraries through Interlibrary Loan. It will be in your account for **30** days. After 30 days, the PDF will be permanently deleted.

If you received the wrong item, or if there are any other problems with the PDF (such as missing pages or unclear images), **please contact the**Interlibrary Loan Office. We will ask the supplier for a corrected copy.

Interlibrary Loan Office AskILL@udel.libanswers.com

NOTICE: WARNING CONCERNING COPYRIGHT RESTRICTIONS

The copyright law of the United States (Title 17, United States Code) governs the making of photocopies or other reproductions of copyrighted material.

Under certain conditions specified in the law, libraries and archives are authorized to furnish a photocopy or other reproduction. One of these specified conditions is that the photocopy or reproduction is not to be "used for any purpose other than private study, scholarship, or research." If a user makes a request for, or later uses, a photocopy or reproduction in excess of "fair use," that user may be liable for copyright infringement.

This institution reserves the right to refuse to accept a copying order if, in its judgment, fulfillment of the order would involve violation of copyright law.

Articles received through Interlibrary Loan may not be redistributed.



Rapid #: -17678234

CROSS REF ID: 824436

BOS:: Main Library LENDER:

DLM:: Main Library **BORROWER:**

TYPE: Article CC:CCG

JOURNAL TITLE: Journal of environmental chemical engineering

USER JOURNAL TITLE: Journal of Environmental Chemical Engineering

The removal of polycyclic aromatic hydrocarbons (PAHs) from marine sediments using persulfate over a nano-sized iron composite of magnetite and carbon black activator ARTICLE TITLE:

ARTICLE AUTHOR: Hung, Chang-Mao

8 VOLUME:

ISSUE: 5

MONTH:

YEAR: 2020

PAGES: 104440-

ISSN: 2213-3437

OCLC #:

Processed by RapidX: 6/16/2021 7:20:21 AM

This material may be protected by copyright law (Title 17 U.S. Code)

ELSEVIER

Contents lists available at ScienceDirect

Journal of Environmental Chemical Engineering

journal homepage: www.elsevier.com/locate/jece





The removal of polycyclic aromatic hydrocarbons (PAHs) from marine sediments using persulfate over a nano-sized iron composite of magnetite and carbon black activator

Chang-Mao Hung ^a, Chin-Pao Huang ^b, Su Shiung Lam ^c, Chiu-Wen Chen ^a, Cheng-Di Dong ^{a,*}

- a Department of Marine Environmental Engineering, National Kaohsiung University of Science and Technology, Kaohsiung City, Taiwan
- ^b Department of Civil and Environmental Engineering, University of Delaware, Newark, USA
- ^c Pyrolysis Technology Research Group, Institute of Tropical Aquaculture and Fisheries (Akuatrop) & Institute of Tropical Biodiversity and Sustainable Development (Bio-D Tropika), Universiti Malaysia Terengganu, 21030, Kuala Terengganu, Terengganu, Malaysia

ARTICLE INFO

Editor: Z. Wen

Keywords: Fe₃O₄-CB persulfate polycyclic aromatic hydrocarbons sediments

ABSTRACT

The presence of polycyclic aromatic hydrocarbons (PAHs) in sediments is a potential eco-environmental health risk. Fe₃O₄-carbon black (FCB) nanocomposite was synthesized by a simplified precipitation method and used to activate persulfate (PS) for the degradation of PAHs in contaminated marine sediments. The carbon black was formed by amorphous non-graphite and the Fe₃O₄ composed of magnetite of cubic crystal structures. FCB exhibited typical ferromagnetic characteristics and high degradation of PAHs in marine sediments via PS oxidation. The pseudo–first–order rate constant of PAHs degradation significantly increased with PS dosage but decreased with increase in pH from 3 to 9. Langmuir-Hinshelwood model described the kinetics of PAHs degradation well. The observed rate constant, k_{obs} (1.8 × 10⁻² h⁻¹), at Σ [PAH]: [PS] = 1:10⁴ (the optimal condition) was almost 2.7 times that of 1:1 (k_{obs} = 6.6 × 10⁻³ h⁻¹). At the PS concentration of 2 × 10⁻⁴ M (or a Σ [PAH]: [PS] = 1:10), pH 3, and 3 g/L of FCB, the FCB/PS system exhibited 94, 97, 94, 98, and 93% degradation of total PAH (Σ [PAH]), PY, FLU, CH, and PH, respectively, while the highest PAH degradation was 99, 98, 97, and 97%, respectively, for 6–, 5–, 4– and 3–ring PAHs. The presence of Fe²⁺/Fe³⁺ redox pairs greatly enhanced the catalytic capacity of FCB leading to an increase in PAH degradation. Electron paramagnetic resonance (EPR) spectroscopy revealed SO₄-• and HO• radicals as major reactive species for PAHs degradation in FCB/PS system. Results clearly indicated the great potential of FCB for remediation of PAHs contaminated marine sediments.

1. Introduction

The contamination of natural water systems and marine sediments by persistent hazardous organic compounds such as polycyclic aromatic hydrocarbons (PAHs), is a major eco-environmental and human health problem that has attracted great public concerns (Dong et al., 2017a; Du and Jing, 2018; Ontiveros-Cuadras et al., 2019; Bortone et al., 2020). Because of the high hydrophobicity and solid/liquid partition coefficient, and low water solubility and volatility, PAHs tend to be adsorbed and accumulated intensively in aquatic sediments and become one of the most widely spread global contaminants (Maletić et al., 2019; Merhaby et al., 2019). The discharge of PAHs via anthropogenic processes to the natural ecosystems has imposed significant adverse effects on aquatic life and human health with respect to bioaccumulation,

carcinogenicity, mutagenicity, and teratogenicity (Han et al., 2019; Meng et al., 2019). Therefore, it is of great urgency to develop effective *ex-situ* technology for the removal of PAHs from contaminated dredged marine sediments (Dong et al., 2018a, b; Giovanni et al., 2018; Ahmad et al., 2019; Bianco et al., 2020; Wang et al., 2020).

Numerous sulfate radical-based chemical oxidants, such as sodium persulfate ($Na_2S_2O_8$; PS), potassium peroxymonosulfate (KHSO₅; PMS), and potassium peroxydisulfate ($K_2S_2O_8$; PDS) have been employed for the degradation of bio-refractory organic chemicals from contaminated sediments owing to their strong oxidation ability, cost-effectiveness, and large application capability (Matzek and Carter, 2016; Ghanbari and Moradi, 2017; Song et al., 2019). The PS-based system is a symmetric oxidant composed of two groups of SO_3 — in an O-O bond, which dissociates in water to form $S_2O_8^2$ —. It is a strong and relatively stable

E-mail address: cddong@nkust.edu.tw (C.-D. Dong).

^{*} Corresponding author.

oxidant and a promising option for rapid degradation of a broad range of organic compounds in aqueous media through formation of highly reactive radical species such as SO_4 - $^{\bullet}$ ($E_0 = 2.5$ -3.1 V) and HO_{\bullet} ($E_0 = 2.4$ -3.0 V). These radicals can efficiently degrade specific contaminants in most environmental media including sediments to harmless products such as CO_2 and H_2O (Hung et al., 2016a; Liu et al., 2016; Dong et al., 2017b; Zhang et al., 2020a, 2020b; Hung et al., 2020a).

However, the use of PS as an oxidant has kinetic limitations due to slow reactivity (Peluffo et al., 2016). To enhance the effectiveness of PS, activators must be used to generate SO₄-* radicals which has high reactivity. Iron-containing solid materials such as Fe₃O₄ magnetic nanoparticles can catalyze PS decomposition to produce highly reactive SO₄-• radicals (Hung et al., 2016b). Sulfate radical is known to have ability to efficiently destroy organic contaminants, mainly through electron transfer mechanisms in sediment decontamination and due to their low cost, biocompatibility, environmental friendliness, and easy separation due to its unique magnetic properties (Dong et al., 2019a, b). However, magnetic nanoparticles agglomerate rapidly, owing to magnetic interaction, crystal face attraction, and being easily oxidized to ferric oxide, becomes a challenge to their wide field applications. Hence, most studies have focused on functional modification of Fe₃O₄ nanoparticles to further improve its catalytic capacity (Dong et al., 2019c; Kamari and Shahbazi, 2020).

Recently, various carbon materials have been studied for possible applications in environmental remediation (Dong et al., 2018a, b; Zhu et al., 2019; Qin et al., 2020). In particular, the PS-based oxidation system using carbon material activators such as graphene, carbon nanotubes, and derivatives exhibited enhanced catalytic degradation of organic contaminants. Wu et al. (2019) studied the removal of cyanobacteria in water using high frequency and low intensity ultrasound in combination with Fe₃O₄/multi-wall carbon nanotubes (MWCNTs) and PS system and reported that both ${\rm SO_4}^{-\bullet}$ and ${\rm \bullet OH}$ radicals played critical roles in the inactivation of cyanobacterial cells. Yin et al. (2019) reported that high-performance reduced graphene oxide nanosheet-Fe₃O₄ magnetic nanoparticles (rGO-Fe₃O₄) composite improved the norfloxacin (NOF) degradation significantly by increasing the concentration of Fe³⁺ in the solution, which led to the continuous generation of reactive species such as SO₄-•, HO•, and ¹O₂ in a manner similar to that of the Fenton-type reaction. However, most of the carbon materials used were high cost and thus great limitation in practical applications. Carbon black (CB) has attracted considerable attentions as promising support materials for metal and metal oxides. CB has strong mechanical and thermal stability in harsh environments, including basic or acidic media (Ren et al., 2019). Furthermore, because of its porous structure, abundant surface functional groups, low cytotoxicity and high specific area, CB has high catalytic capacity toward the degradation of organic compounds in sediments (Dong et al., 2019d). The chemical structure and microporosity of CB strongly influenced the sorption/desorption characteristics and chemical degradation of PAHs (Kołtowski et al., 2020). Dimitriadou et al. (2020) studied the removal of the drug diclofenac (DCF) by a CB-activated PS system and reported that SO₄-* and HO* were the major species responsible for complete DCF degradation. Moreover, magnetic Fe₃O₄ nanoparticles surface coated with CB has been reported to be effective in preventing the aggregation and further heterogeneous oxidation of hazardous chemicals because of its magnetic property and high biocompatibility (Dong et al., 2020a). Li et al. (2019) studied the treatment of PAH-contaminated water using a Fe-Mn binary oxide modified biochar (Fe-Mn/biochar) process, and reported that the Fe-Mn/biochar/PS photo-Fenton system significantly reduced the naphthalene (NA) content in contaminated soils. Pi et al. (2019) studied the removal of the antibiotic tetracycline (TC) using PS activated by biochar supported nano magnetite particles, and reported a TC degradation of greater than 92%, with SO₄-• and •OH radicals playing dominant roles in the reaction. The enhanced catalytic reactivity was caused by the reduction-oxidation couples of Fe²⁺/Fe³⁺ and the abundant surface oxygen-containing groups, preceded by a strong

electrostatic attraction between TC molecules and magnetite catalyst.

In this study, a magnetic FCB nanocomposite was prepared by a simplified precipitation method. The present study aimed at developing FCB process for removing PAHs from marine sediments. The influence of various parameters including PS concentration, FCB dosage, and initial pH on PAHs degradation in marine sediments were evaluated. The FCB was fully characterized using transmission electron microscopy (TEM), Raman, Fourier—transform infrared (FTIR) spectroscopy, X-ray diffraction (XRD), vibrating sample magnetometry (VSM), zeta potential, X-ray photoelectron spectroscopy (XPS), cyclic voltammetry (CV), linear sweep voltammetry (LSV) and electron paramagnetic resonance (EPR) spectroscopy. Additionally, FCB were studied using three-dimensional excitation—emission fluorescent matrix (3D—EEFM) spectroscopy technology to gain insight into the dominant fluorescent components. Finally, it was to establish the mechanism of PAH degradation PS over the FCB composite.

2. Experimental

2.1. Sediment collection

Sediments, at the top 0 to 15 cm depth, were sampled from Kaohsiung Harbor, Taiwan. Sediment samples were scooped into glass bottles, pre-washed with *n*-hexane, capped immediately and kept frozen while been transported to the lab. The sediments were dried in the air for 7 days, then homogenized and ground to passing a sieve (2-mm opening). Afterward, samples passing through 0.5-mm sieve were homogenized using a mortar and pestle, and then freeze-dried for 72 h. The sediment sample contained 34% of sand, 61% of silt, and 5% of clay (Table S1). The analytical results were reported on a dry-weight basis.

2.2. Chemicals and reagents

Sodium persulfate ($Na_2S_2O_8$) was obtained from Sigma-Aldrich Co. Ltd. (St. Louis, USA), n-hexane (99.8%, HPLC grade), acetone, and methanol were received from Merck (Darmstadt, Germany). Standards of 16 PAHs in 80 mg/L mixture solution, deuterated PAH internal standard solution at 4000 mg/L, and surrogate standard solutions at 2000 mg/L were obtained from AccuStandard, Inc. (New Haven, CT, USA). The ultrapure water used in the experiment was purified by a Milli-Q water purification system (Millipore, MA, USA).

2.3. Catalyst preparation

The magnetic Fe $_3O_4$ particles were prepared by co-precipitation, using FeCl $_3 \bullet 6H_2O$ and FeCl $_2 \bullet 4H_2O$ at [Fe $^3+$] : [Fe $^2+$] = 2:1 following Hung et al. (2016b) with slight adjustments. The above iron solution was added ammonia (1.0 M) dropwise until the pH exceeded 9.0 at room temperature while being stirred vigorously, then heated for 4 h at 80 °C in an oven to dryness. Washed the solids with adequate amount of deionized water till reaching a neutral supernatant pH. Freeze-dried washed solids till black particles which were magnetite products.

The magnetized FCB nanocomposite catalyst was synthesized using a wet-chemistry approach. Briefly, before Fe $_3O_4$ deposition, placed 100 mg of Vulcan XC–72 CB substrate (Uni-Onward Corp., Kaohsiung, Taiwan) in 2 M HNO $_3$ solution (J.T.Baker, PA, USA), refluxed for 2 h, then filtered to collect the solids. Washed the solids with DI water then dried at 60 °C for 360 min in an oven. Afterward, dispersed the FCB composite (containing 5 wt% of Fe $_3O_4$) with CB in hydroxypropyl cellulose (Acros, NJ, USA) solution. Homogenized the mixture in a sonicator for half of an hour followed by mechanical stirring for two hours. The solids were collected after being heated at 200 °C, then calcinated again at 300 °C under nitrogen gas for 6 hours. The final particle products were used in all experiments.

2.4. PAH degradation experiments

Experiments began by placing 1 g of sediments and 25 mL of PS solutions in glass flasks (40 mL volume) at different [PAHs] to [PS] molar ratio from 1:1 to 1:10⁴. Thereafter, the FCB was added to each of the sample vials and then gently shaken for 30 s before being placed in a water bath shaker (SB-9D, Taiwan Hipoint Corporation, Kaohsiung, Taiwan) for continuingly shaken at a speed of 200 rpm for 24 h. All experiments, including controls, were triplicate. At the end of each experiment, a given amount of potassium iodide (KI) was added to quench the PS degradation reaction. The residual PAHs were extracted into 1:1(v/v) acetone:n-hexane, v/v under sonification. PAH concentration was determined by gas chromatography-mass spectrometry (GC-MS). Analysis of the 16 PAHs of the US EPA priority pollutant including naphthalene (NA), acenaphthylene (ACY), acenaphthene (ACE), fluorene (FL), phenantrene (PH), anthracene (AN), fluoranthene (FLU), pyrene (PY), benzo[a]anthracene (BaA), chrysene (CH), benzo [b]fluoranthene (BbF), benzo[k]fluoranthene (BkF), benzo[a]pyrene (BaP), indeno[1,2,3-cd]pyrene (IP), dibenzo[a,h]anthracene (DA), and benzo[g,h,i]pervlene (BP).

2.5. Analysis of PAHs

The residual PAHs concentration in the sediment extracts were analyzed using gas chromatograph (Model 6890; Agilent Technologies, USA) equipped with a mass selective detector (Model 5975; Agilent Technologies, USA) and an Agilent 7683B split/splitless injector (1 min splitless time; 60 mL/min flow rate) in selected ion monitoring (SIM) mode. The injector temperature was 300 °C. The ion source and transfer line temperatures were 230 and 280 °C, respectively. PAH were separated on a GC–MS with HP–5MS capillary column (30 \times 0.25 mm) with 0.25 μm film thickness (Hewlett-Packard, Palo Alto, CA, USA). Helium was the carrier gas operated at 1 mL/min flowrate. The initial column temperature was 40 °C @ 1 min, increased to 120 °C @ 25 °C/min, then 160 °C @ 10 °C/min, and finally 300 °C @ 5 °C/min. The correlation coefficient (R²) was 0.98 for each calibration curve.

2.6. Characterization of FCB

The surface morphology of FCB composites was analyzed using TEM (CM-200 Twin; Philips, Netherlands). Raman spectroscopy analysis was conducted using a visible Raman system (Nanofinder 30; Tokyo Instruments, Japan) with a 632.8 nm He-Ne laser. FTIR spectra were obtained (FT-700; Horiba, Japan) at a scan number of 32 and spectral resolution of 4 cm⁻¹. XRD curves were recorded using a CuKα radiation source (Diano-8536 diffractometer). A superconducting quantum interference device (SQUID) magnetometer (MPMS-XL7; Quantum Design, USA) was used to study the magnetic properties of FCB composite. Zetasizer Nano ZS90 (Malvern Instruments, Worcestershire, UK) was used to measure the surface charge of FCB as a function of pH, from 3 to 11, being adjusted with HNO₃ (0.1 M) or NaOH (0.1 M). Chemical composition analysis was performed using XPS (AXIS Ultra DLD; Kratos Analytical Ltd., Manchester, UK). The cyclic voltammetry (CV) and linear sweep voltammetry (LSV) measurements were conducted at room temperature using an electrochemical analyzer (CHI 6081D, USA) using a three-electrode electrochemical cell to investigate the electrochemical behavior of the FCB (Hung et al., 2020b). The samples were scanned at a rate of 25 mV/s between -2.0 and 2.0 V. Glassy carbon and platinum wire were the working and counter electrode, respectively. Saturated Ag/AgCl electrode was the reference electrode. The supporting electrolyte was Na₂SO₄ (0.5 M). The three-dimensional excitation–emission fluorescent matrix (EEFM) spectra were obtained using a luminescence spectrophotometer (F-4500; Hitachi, Japan) with a xenon lamp as the excitation source. In this investigation, EEFM comprised 60 segments in excitation wavelength and 60 segments in emission wavelength from the range between 200 to 800 nm, yielding discrete values of fluorescence intensity at 3600 pairs of excitation/emission wavelengths. Spectral subtraction was performed to remove the blank spectra from pure water. 5,5-dimethyl-1-pyrroline N-oxide (DMPO) was used as spin-trapping agent to quantify SO_4 – and HO_{\bullet} by electron paramagnetic resonance spectroscopy (EPR) (Bruker Company, EMX-10/12, Germany). The peak intensity of DMPO–SO₄– and DMPO–HO $_{\bullet}$, after background noise correction, gave the concentration of SO_4 – and HO_{\bullet} , respectively.

3. Results and discussion

3.1. Surface and physical properties of FCB

Fig. 1a gives the typical TEM image of FCB. The FCB consisted of spherical particles ranging from 10 to 50 nm in size. The presence of nano-sized FCB particles is likely to increase the active sites and improve the catalytic effectiveness. Some degrees of aggregation can be attributed to the static magnetism and surface force between Fe₃O₄ and CB. Fig. 1b shows the Raman spectrum of FCB. Two main D and G peaks at 1359 and 1580 cm $^{-1}$ were observed, assignable to typical amorphous carbons. Two peaks at 665 and 535 cm $^{-1}$ were observed, assignable to typical feature of Fe₃O₄. The large ratio of intensity of D and G peaks (I_D/I_G) of 1.4 indicated surface defective sites on FCB, which could be beneficial to PS activation (Sun et al., 2020).

The FTIR spectra of the various materials were then obtained for wavelengths of $400-4000 \text{ cm}^{-1}$ (Fig. 1c). The samples exhibited several sharp peaks. The first Fe-O band, observed at 445 and 590 cm⁻¹ was correspondent to intrinsic stretching vibrations of the Fe3+O2- and Fe²⁺O²⁻ ions (Alveroğlu et al., 2013; Pi et al., 2019), respectively, implying the formation of chemical bond between the CB and Fe₃O₄ phases. It is possible that mechanical interlocking, as well as columbic interactions, took place between Fe-O bonds and oxygen-containing functional groups (OFGs) present on the surfaces of the FCB (Dong et al., 2019a). In contrast, several major peaks were detected at 1080, 1539, 1657, 1719 and 3442 cm⁻¹, which were related to C-O, carboxylate (-COOH) group, C = C, carboxylic C = O group, and hydroxyl-OH stretching, respectively (Truong et al., 2020). A peak at 1590 cm⁻¹ belonged to the quinonyl and ketone groups. A weak peak at 2358 ${\rm cm}^{-1}$ was attributed to the aliphatic structure. The peak at 1100 cm⁻¹ was due to the surface functional group of carbonyl (-C = O) and C-O-C(Dimitriadou et al., 2020). These results suggest that the obtained FCB contained a large number of aromatic and oxygenic functional groups.

Fig. 1d gives the XRD spectra obtained at 2θ between 10 and 80° . The intense diffraction peaks indicated the cubic crystal structure of Fe₃O₄, at 2θ 30.4°, 35.5°, 53.5°, 57.0°, and 63.0°, attributed to (220), (311), (422), (511), and (440) facets, respectively. No other peaks were observed, suggesting that Fe₃O₄ was the major phase on FCB. There was a weak graphitic diffraction peak (101) at 2θ ~43.5°, representing the relatively stable lamellar crystal structure of graphitic carbon (Dimitriadou et al., 2020). Results verified successful synthesis of FCB with incorporation of Fe₃O₄ in CB.

Fig. 1e gives the magnetic behavior of FCB in magnetic field between -10 and +10 kOe. The $M\!-\!H$ hysteresis curves passed the original point, indicating that the FCB possessed typical superparamagnetic behavior (Kumar et al., 2019). The saturation magnetization of the FCB was 49 emu/g, implying that the FCB exhibited an excellent magnetic response to a magnetic field and thus could potentially be easily separated from the reaction system after completing the catalytic process. Fig. 1f gives the surface charge as a function of pH. The isoelectric point (pH_{IEP}) was 4.6. The result revealed that the FCB had positively charged surfaces at pH < 3 and negatively charged surface at pH 5–11, which was possibly attributed to the ionization of surface OFGs such as carboxyl (–COOH) and hydroxyl (–OH) groups on its surface that decreased the zeta potential.

As shown in Fig. 2a, the survey spectra of FCB exhibited signals relevant to Fe2p, C1s, and O1s, which were observed at binding energies of 714.9, 284.6 and 533.2 eV, respectively. Peaks of Fe2p_{3/2} and Fe2p_{1/2}

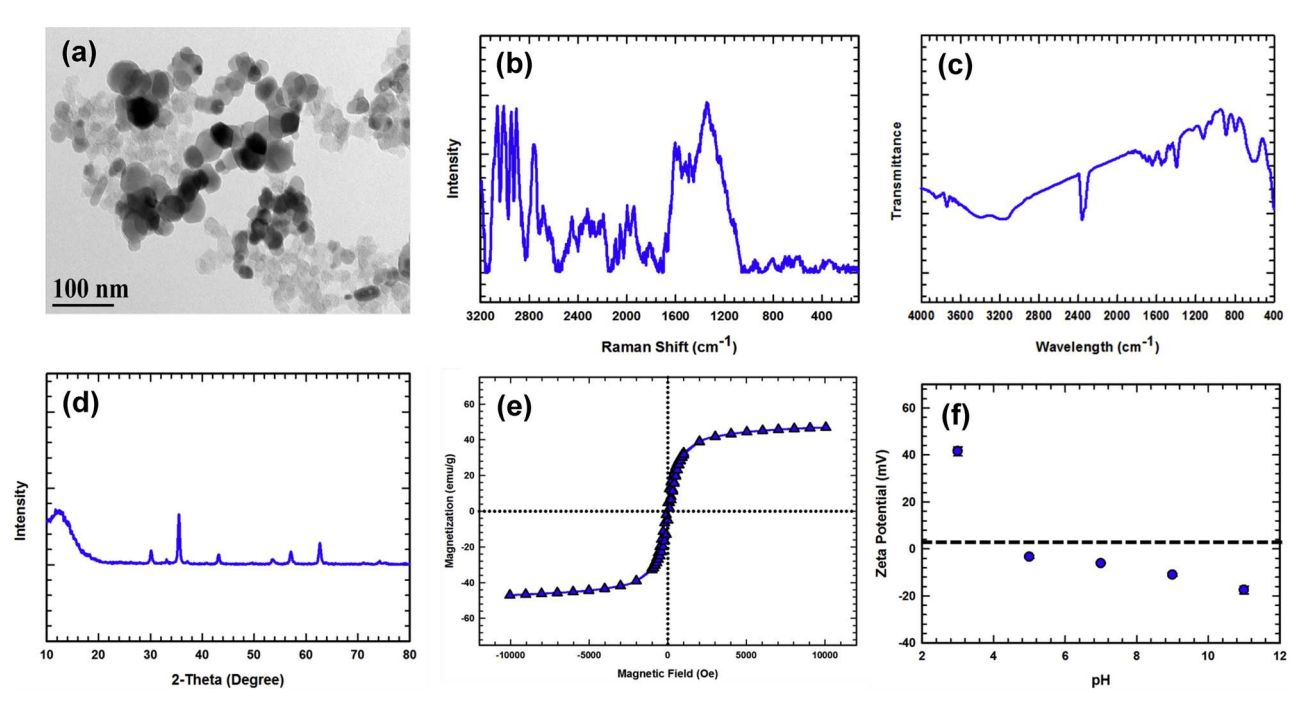


Fig. 1. The (a) TEM images, (b) Raman and (c) FTIR spectra, (d) XRD pattern, (e) magnetic hysteresis loops, (f) zeta potentials of FCB.

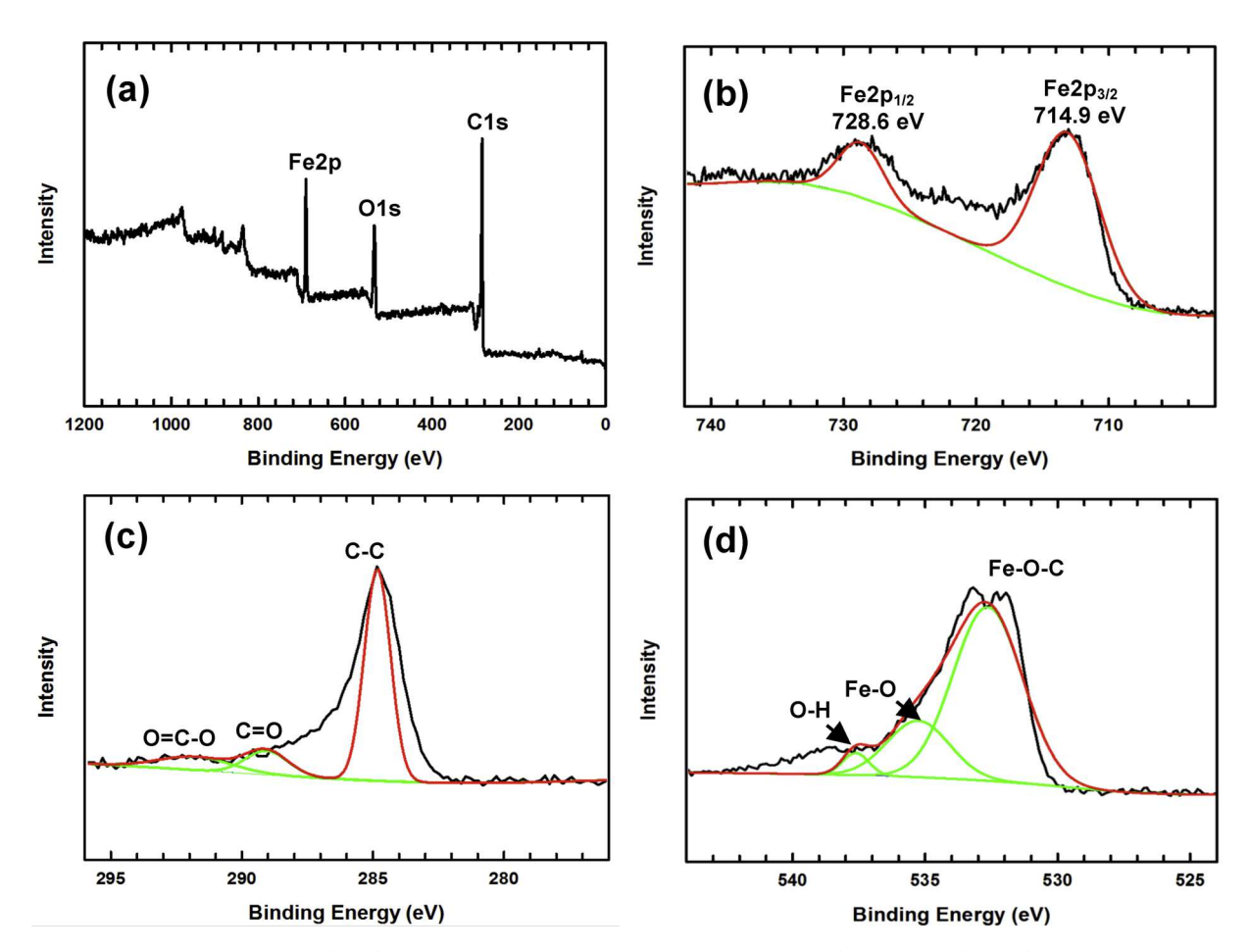


Fig. 2. Wide-scan X-ray photoelectron spectroscopy (XPS) spectrum of FCB (a); Fe2p (b); C1s (c); and O1s (d) XPS spectra.

at 714.9 and 728.6 eV (Fig. 2b) indicated Fe^{3+} and Fe^{2+} , respectively. In addition, the peaks at 284.6, 285.1, 288.1, and 292.3 eV were attributed to C=C, C=C, C=C and C=C0, respectively (Yin et al., 2019)

(Fig. 2c). The three peaks of O1s at 531.2, 535.6, and 537.5 eV were Fe–O–C, oxygen in hydroxyl groups (O–H), and Fe–O, respectively (Fig. 2d), thereby indicating that a surface hydroxylation layer (M–OH)

might form on the FCB. Results of XPS confirmed again the successful deposition of ${\rm Fe_3O_4}$ on CB due to strong association between Fe–O and carbon atoms of CB.

3.2. PAH degradation by FCB-activated PS

3.2.1. Effect of initial PS concentration on PAH degradation

The concentration of PAHs in the untreated sediment was approximately 4,395 \pm 273 ng/g dry weight, which implied that the sediments were at medium to high contamination level by PAH according to Baumard et al. (1998). PY, PH, and FLU were major PAHs components, whereas 4–ring (PY, FLU, CH) and 3–ring (PH) PAHs were the most abundant constituents (58% of total PAH). PY, a symmetrical 4–ring compound, was one of the most abundant PAHs in the environment because of its resistance to biological degradation and high solubility in water (Nayebzadeh et al., 2020). The individual PAHs with the highest concentration was PY (1063 \pm 71 ng/g) followed by PH (595 \pm 75 ng/g).

The degradation of PAHs was observed when the PS dosage was increased from 2×10^{-5} to 2×10^{-1} M (or $\Sigma[\text{PAH}]$: [PS] = $1:10^4$) (Fig. 3a). Result indicated higher PS concentration yield higher PAH degradation. The largest ΣPAH removal was 70% at an PS concentration of 2×10^{-1} M (or a $\Sigma[\text{PAH}]$: [PS] = $1:10^4$), which indicated that more SO_4 –° were generated by PS for the oxidation of PAHs. At lower PS concentration of 2×10^{-5} M (or $\Sigma[\text{PAH}]$: [PS] = 1:1), the PAH removal efficiency was only 18%. The results demonstrated the ability of PS to degrade organic contaminants. Peluffo et al. (2016) reported that at high PS concentrations reactive SO_4 –° and HO• contributed to the

degradation of PAH. ${\rm SO_4}^{-\bullet}$ attack PAHs through electron transfer reaction. The electron–transfer process occurred to form PAH radical cation (PAH $^{\bullet}$), which reacted quickly with H₂O by hydroxyl abstraction or addition to generate (hydroxyl)PAH radicals ((OH)PAH). (OH)PAH could be transformed into different intermediates and was further oxidized to ${\rm CO_2}$ and H₂O (Liu et al., 2018). Generally, the degradation recalcitrant compounds like PAHs requires very vigorous oxidation conditions (Ferrarese et al., 2008). Especially in sediments where the presence of high organic matter content and strong solid matrix requires much strong oxidants and elevated dosage. Results in Fig. 3a indicated that Σ [PAH] removal increased sharply at Σ [PAH]: [PS] 1:10², then tailed off as the Σ [PAH]: [PS] ratio was greater than 1:10³. Further increase in Σ [PAH]: [PS] ratio did not exhibit significant increase in Σ [PAH] removal.

The molecular weight and ring number of PAH species determined the degree of removal of individual PAH. PAHs included hundreds of individual chemicals of two or more fused aromatic rings, namely, the low-molecular-weight (LMW) PAHs (two and three–rings) and the high-molecular-weight (HMW) PAHs (four to six–rings). Because of greater water solubility, LMW PAHs were more degradable than HMW PAHs. There were three PAHs (LHW PAH-ACY, HMW PAH-DA, IP) present at relatively low concentrations in sediments. The FCB/PS system exhibited 92, 45, 63, and 36% of degradation of PY, FLU, CH, and PH, respectively, at the highest PS concentration of 2×10^{-1} M (Fig. 3b). The degradation of PAHs was 94, 66, 58, and 95% for the 3–, 4–, 5– and 6–ring PAHs, respectively (Fig. 3c). The degradation rate constants of PAHs were calculated by fitting the experimental data to a pseudo-first-order kinetic model (explained in detail in the Supporting Information

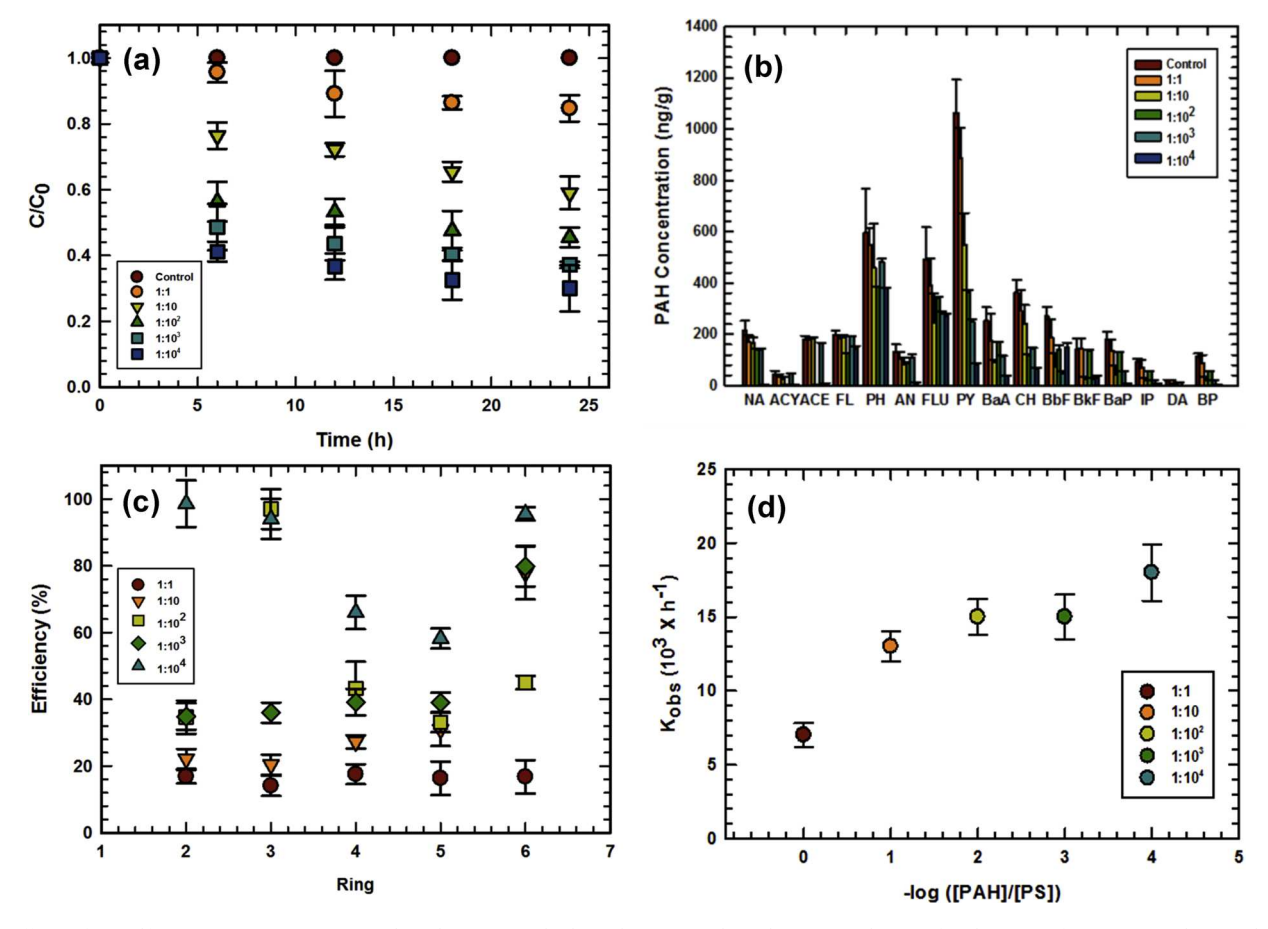


Fig. 3. Effects of persulfate (PS) concentration on polycyclic aromatic hydrocarbon (PAH) degradation. (a) Change of molar ratio of \sum PAH: PS. (b) Distribution of PAH degradation products at 24 h. (c) Degradation efficiency of PAH as a function of ring number. (d) Rate constant of PAH degradation. Values are expressed as mean \pm standard deviation of triplicate samples. Experimental conditions: sediment = 1.00 g, reaction volume =40 mL, T =25 °C, pH₀ = 6.0, molar ratio of \sum PAH: [PS] = 1:10°-10⁴.

S3: Derivation of kinetics equation). The slope of a linear $\ln(C/C_0)$ vs. time (t) plot gave the rate constant (k_{obs}) , where C_0 and C were initial and final PAH concentrations, respectively. As shown in Fig. 3d, k_{obs} $(1.8 \times 10^{-2} \, h^{-1})$ at $\Sigma[PAH]$: $[PS] = 1:10^4$ (the optimal condition) was almost 2.7 times that of 1:1 $(k_{obs} = 6.6 \times 10^{-3} \, h^{-1})$, because of the abundant SO_4 - $^{\bullet}$ and HO_{\bullet} available for reaction with most PAHs contaminants.

3.2.2. Effect of FCB dosage on PAH degradation

FCB dosage (2.0-7.0~g/L) had a significant influence on PAH degradation in the FCB/PS system. Fig. 4a shows that the amount of PAH degradation with PS alone was about 41% of PAHs over 24 h, indicating that PS could not effectively oxidize PAHs without an activator. In contrast, PAHs degradation occurred rapidly when the FCB dosage was increased from 2.0 to 7.0 g/L. These results indicated that the PAHs degradation rate was increased in the order of 3.0 > 2.0 > 7.0~g/L, indicating that the interaction between FCB and PS promoted PAHs degradation. At the FCB dose of 3.0~g/L, the degradation of PAHs reached 82% (Fig. 4a).

The increase in FCB dose accelerated the generated SO_4 — and HO_{\bullet} from the activation of PS by FCB for PAHs degradation revealing that electron transfer occurred from the iron species and caused the presence of abundant redox-active centers of FCB (Zhang et al., 2020a, 2020b). Moreover, PAH degradation was 99, 70, 77, and 91% for PY, FLU, CH, and PH, respectively, when FCB dose was increased to 3.0 g/L (Fig. 4b). At this dosage, the highest PAH degradation was 95, 92, 87, and 93%, respectively, for 6–, 5–, 4– and 3–ring PAHs (Fig. 4c).

The Langmuir-Hinshelwood mechanism of heterogeneous catalysis

assumed rapid adsorption of reactants (i.e. PS and PAHs) on the catalyst surface (Supporting data S3). The observed rate constants, k_{obs} , were 2.0×10^{-2} , 2.2×10^{-2} , and 2.1×10^{-2} h⁻¹ at FCB dosages of 2.0, 3.0, and 7.0 g/L, respectively (Fig. 4d). Results showed that the maximum k_{obs} was at the FCB dosage of 3.0 g/L, which was in accordance with Eq. (S15). Therefore, with increasing FCB loading of 3.0 g/L, more available surface active sites would take part in the PS catalytic reaction to generate reactive species in sediment. The activation behavior of PS to produce SO₄–• and HO• may be ascribed to the possible existence of a π – π interaction between the aromatic structures of CB and Fe₃O₄ in the FCB/PS system (Truong et al., 2020). These results suggested that FCB was an efficient PS activator for the degradation and mineralization of electron-rich PAHs, where FCB acted as an electronic medium to accelerate electron transfer.

3.2.3. Effect of pH on PAH degradation

The PAHs degradation in the FCB/PS system as a function of initial pH was studied. In general, the initial pH played an important role in PS activation. Fig. 5a shows significant PAH degradation of 94 and 82% in 24 h, at pH 3.0 and 6.0, respectively. PAHs removal was slightly decreased from 82% to 80% when pH was increased from 6.0 to 9.0. These results demonstrated that PAHs degradation by FCB–activated PS was more favorable under relatively acidic and neutral conditions. Eqs. (1) and (2) indicate the possibility of accelerating the decomposition of PS under acidic conditions to generate SO_4 - $^{\bullet}$:

$$S_2O_8^{2-} + H^+ \to HS_2O_8^-$$
 (1)

$$HS_2O_8^- \to SO_4^{\bullet -} + SO_4^{2-} + H^+$$
 (2)

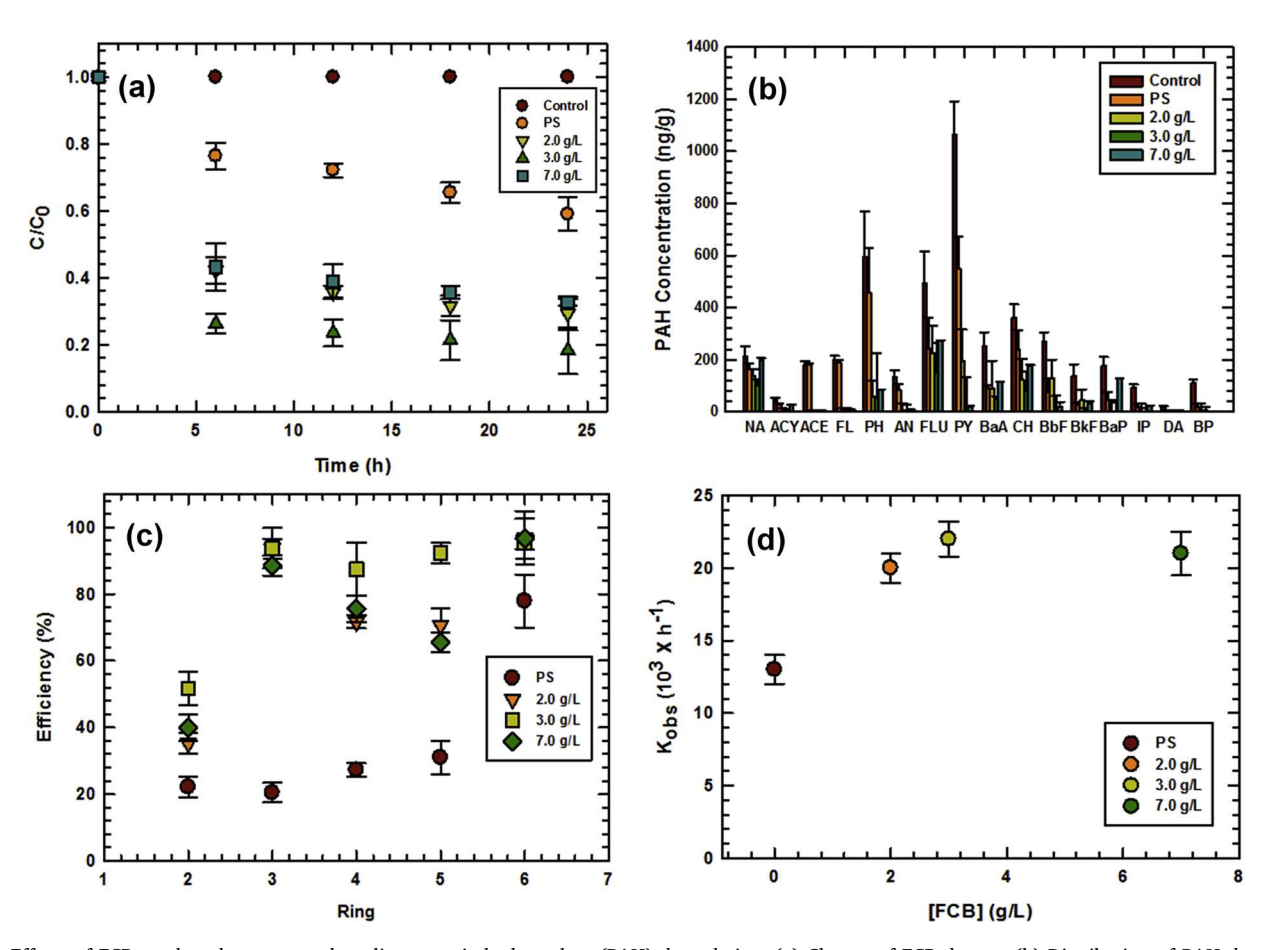


Fig. 4. Effects of FCB catalyst dosage on polycyclic aromatic hydrocarbon (PAH) degradation. (a) Change of FCB dosage. (b) Distribution of PAH degradation products at 24 h. (c) Degradation efficiency of PAH as a function of ring number. (d) Rate constant of PAH degradation. Values are expressed as mean \pm standard deviation of triplicate samples. Experimental conditions: sediment = 1.00 g, reaction volume =40 mL, T =25 °C, pH₀ = 6.0, [PS] = 2 × 10⁻⁴ M, molar ratio of \sum PAH : [PS] = 1:10.

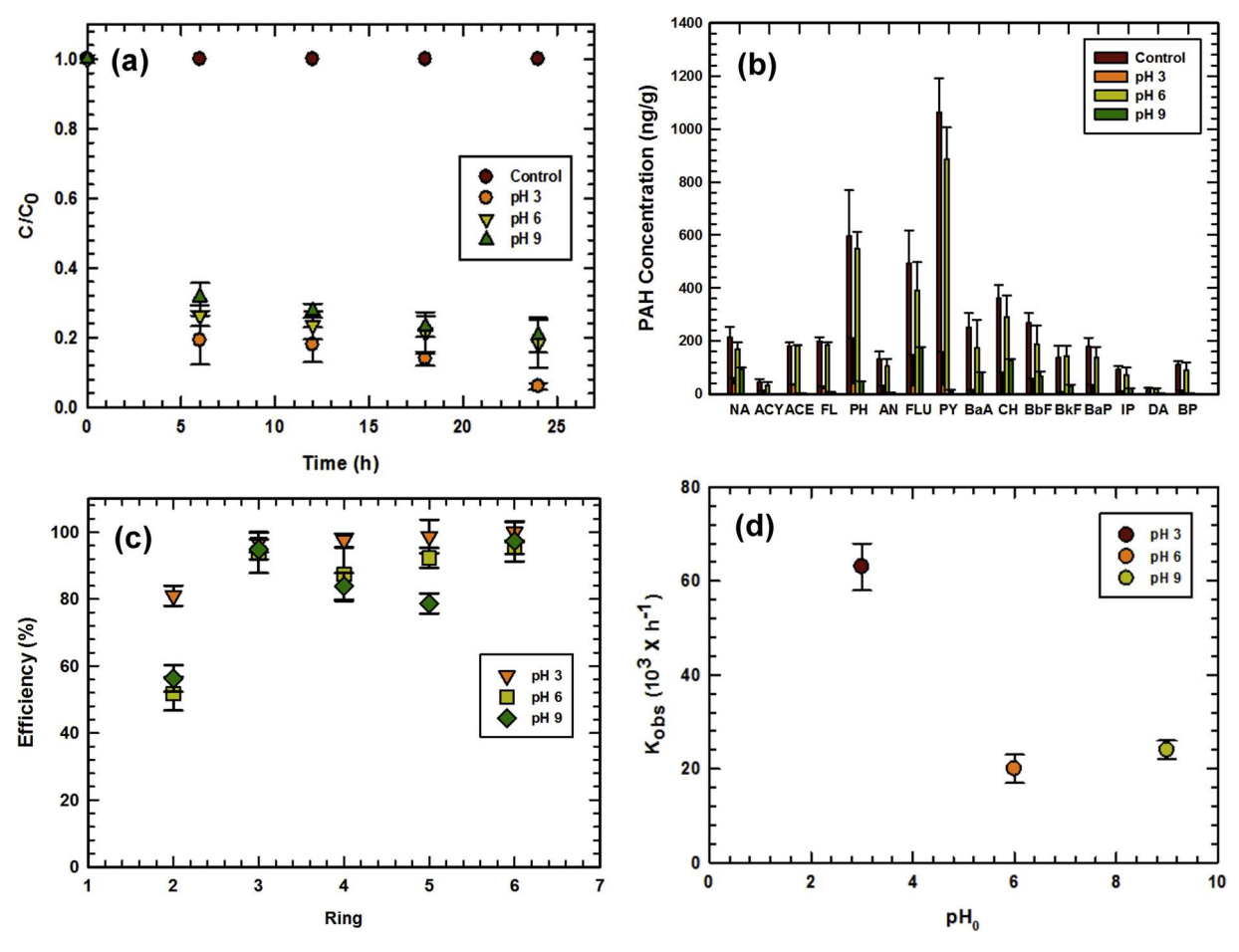


Fig. 5. Degradation of polycyclic aromatic hydrocarbon (PAH) as a function of initial pH in the presence of FCB catalyst. (a) Change of initial pH. (b) Distribution of PAH degradation products at 24 h. (c) Degradation efficiency of PAH as a function of ring number. (d) Rate constant of PAH reduction. Values are expressed as mean \pm standard deviation of triplicate samples. Experimental conditions: sediment = 1.00 g, reaction volume =40 mL, T = 25 °C, [FBC] = 3.0 g/L, [PS] = 2 × 10^-4 M, molar ratios of \sum PAH: [PS] = 1:10.

However, FCB may hydrolyze to form Fe(OH)2 precipitate under neutral or alkaline conditions, which could decrease the activation performance. Moreover, SO₄-• and HO• were produced through PS reaction with H₂O and OH⁻ under alkaline or neutral conditions. The pH of the sediment was well buffered by PS (Danish et al., 2017). Therefore, no apparent inhibition of PAHs degradation was observed at pH₀ 9.0, indicating that the FCB/PS system could function over a wider pH range. The optimal pH of 3.0 yielded the greatest degradation of 97, 94, 98, and 93% for PY, FLU, CH and PH, respectively (Fig. 5b). At the optimal initial pH of 3.0, the highest PAHs degradation was 99, 98, 97, and 97%, respectively, for the 6-, 5-, 4- and 3-ring PAHs (Fig. 5c). The observed rate constant, k_{obs} , was 6.3×10^{-2} , 2.0×10^{-2} , and 2.4×10^{-2} h⁻¹ for pH₀ values of 3.0, 6.0, and 9.0, respectively (Fig. 5d). The results suggested that a decrease in pH favored PAHs degradation, which was consistent with previous results of Dong et al. (2019e). The relatively higher degradation at pH 3.0 could be ascribed to the better adsorption of PAHs on FCB (Liu et al., 2020). The results clearly indicated that FCBcatalyzed PS oxidation was applicable in the acidic to neutral pH region, without precipitating iron, which was superior to the conventional Fenton process. Since SO₄-• was stable under acidic condition, pH affected PS activity greatly. The dissolution of Fe₃O₄, yielding Fe²⁺ and Fe³⁺, increased the activation of PS and generation of SO₄-• and HO•. Excessive Fe²⁺ or Fe³⁺ enhanced the generation of SO₄-• and HO• because of faster electron transfer reactions, thus leading to an increase in PAH degradation. Moreover, CB acted as an electron shuttle to mediate electron transfer reactions in Fenton-like systems. Electrostatic force, hydrogen bonding, and complex formation were likely to be responsible for the oxidation reaction of PAHs in the FCB/PS system. Consequently, controlling the FCB concentration could mitigate its inhibitory effects on SO₄-• and HO• generation. The oxidation capacity of SO₄-• and HO• may decrease with an increase in pH. Alkaline pH increased the HO. scavenging reaction. Moreover, pH played an important role on the adsorption of PAHs and the catalysis efficiency of FCB (Ahmad et al., 2019). The FCB/PS system was pH-dependent and PAHs degradation was most efficient over the range of pH between 3.0 and 9.0. Furthermore, salinity or ionic strength is the predominant factor determining the distribution of PAH in marine sediments (Zhang et al., 2020a, 2020b). Further research focusing on the impact of salinity on the catalytic capability of FCB toward the degradation of PAHs by PS under various water chemistry conditions is ongoing. Pilot scale studies on the ex-situ treatment of PAH-contaminated marine sediments as affected by pH, temperature and salinity (ionic strength) are being conducted in our laboratory.

3.3. Mechanisms for PS activation and PAH degradation by FCB

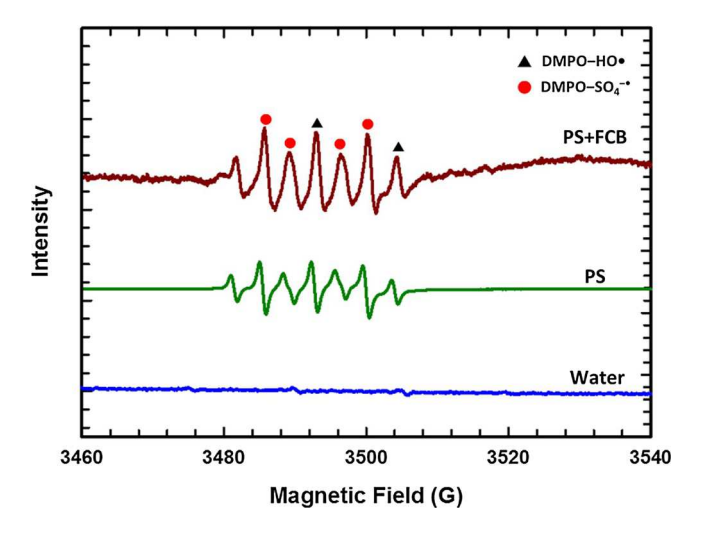
Fig. S1 presents the electrochemical characteristics of FCB. The fresh FCB composite exhibited a highly reversible redox capacity and oxidative current density at scan rate of 100 mV/s (Fig. S1a). The distorted voltammetric redox peaks at -0.4 and 0.5 V represented the reversible ${\rm Fe}^{2+}/{\rm Fe}^{3+}$ redox pair. The peak at 1.4 V was the one-way oxidation of ${\rm Fe}^{2+}\to{\rm Fe}^{3+}$ (Dong et al., 2020b). These results suggested that the reversible redox ability of the FCB played a key role in maintaining good catalytic performance. The LSV curve revealed again that the peak at

0.5~V was the reversible Fe $^{2+}$ /Fe $^{3+}$ redox couple (Fig. S1b). The results suggested that FCB promoted PS activation for PAH degradation. PAH was adsorbed by FCB catalyst prior to the oxidation–reduction reaction occurring at FCB active sites.

Fig. 6a shows fluorescence peaks of the three-dimensional EEFM for a fresh FCB; four significant excitation/emission plots were generated at 220/300 (Peak I), 230/340 (Peak II), 270/310 (Peak III) and 320/ 380 nm (Peak IV). Fig. 6b shows the fingerprint of the EEFM for FCB after the activity test; three substantial excitation/emission plots at 220/ 300 (Peak I), 230/340 (Peak II) and 270/340 nm (Peak V) were observed. Based on the previous literature (Siwach and Sen, 2008; Dong et al., 2017a; Rajapaksha et al., 2019; Yang et al., 2019a; Yang et al., 2019b), peaks I and II, III, IV and V were assigned to Fe₃O₄ nanoparticle, terrestrial condensed fulvic acid, and humic acid-like and typical protein-like containing tryptophan and tyrosine components, respectively. It was obvious that peaks III and IV disappeared in the used FCB, and that two peaks (I and II) could still be observed. This result was similar to that reported by Siwach and Sen (2008), who determined that iron nanoparticles at different excitation wavelengths (λ_{ex}) in the range 220–280 nm provided fluorescence emission at 303 nm for two different ranges of 220-250 nm and 255-280 nm. Moreover, the difference of excitation/emission plot between fresh and used FCB was ascribed to the metal-enhanced fluorescence effect, which indirectly indicated the presence of surface functional groups and surface energy traps that became emissive upon stabilization as a result of surface passivation of the used FCB (Hung et al., 2016a; Hung et al., 2016b). Therefore, the presence of the dominant fluorescence components Fe₃O₄ nanoparticles and CB contributed to the formation of active sites which might accelerate the degradation of PAHs. This result suggested that the adsorption via π - π interaction and hydrogen bonding of large condensed fluorescent structures with enriched carboxylic groups was favored (Truong et al., 2020). However, the disappearance of peak II, IV, and V indicated that the main functional groups had been changed by the PS oxidization and that the numbers of conjugated double bonds, condensed structures, and aliphatic, aromatic carbons, as well as the amount of DOM had been decreased, which may directly affect the composition and characteristics of the FCB (Yang et al., 2019a; Yang et al., 2019b). Furthermore, the function groups on CB surface, specifically, -C = O, -COOH, and -OH, were the active sites that interacted with Fe to form Fe-O-C and Fe-O complexes (Fig. 2d) which facilitated electron transfer between the FCB surface and PS responsible for the catalytic activation of PS for successful degradation of (Lu et al., 2020). The positively charged FCB at pH 3 might easily bind with negatively-charged aromatic compounds

with conjugated double–bonds (Fig. 1f). These results could provide some information on the interaction mechanisms between $\rm Fe_3O_4$ and CB on promoting PAHs degradation.

EPR was used to detect free radicals from PS activated by FCB (Fig. 7). No peaks were observed when adding DMPO to pure water, which implied no capture of spins. The addition of DMPO to PS solution vielded the signal of 5,5-dimethylpyrrolidone-(2)-oxyl-(1) (DMPOX). Two radical adducts were detected when FCB, DMPO, and PS were present together. The dominant signal was ascribed to DMPO-SO₄-•, indicating that SO₄-• was generated in the FCB/PS system and participated at the degradation of PAHs. Additionally, another weaker signal was ascribed to DMPO-SO₄-•, which indicated the contribution of SO₄-• to PAHs degradation. These results demonstrated that the FCB activation of PS generated a large amount of SO₄-•. It is suggested that FCB with a higher oxidation ability could weaken the S-O bond of adsorbed PS, thus promoting the decomposition of PS into SO₄-• (Wang et al., 2018). Breakage of S-O bonds on the surface of the FCB produced active oxygen (O_{ads}). As adding PS to water leads to the generation of SO₄
and HO because of the cleavage of the O-O bond (Eq. 3). PS could be further decomposed to SO_4 - $^{\bullet}$ and O_2^{\bullet} - in the presence of an activator (Eqs. 4-6) (Lin et al., 2017), which triggered a series of synergistic reactions,



 $\begin{tabular}{ll} Fig. 7. Electron paramagnetic resonance (EPR) spectra of radical adducts trapped by 5,5-dimethyl-1-pyrroline N-oxide (DMPO) of the FCB catalyst. \\ \end{tabular}$

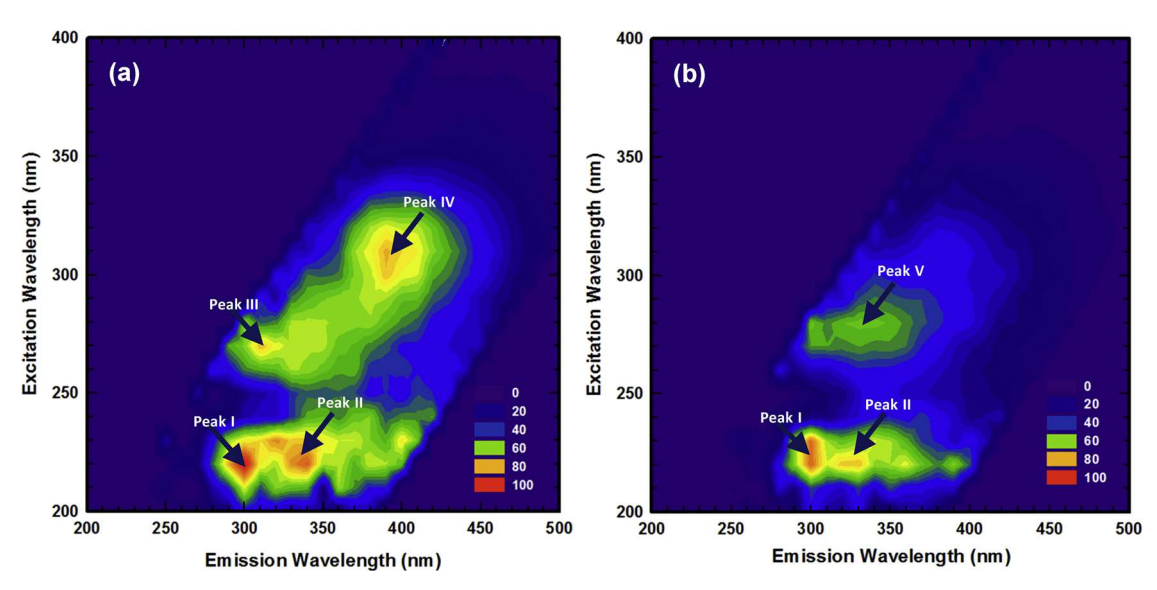


Fig. 6. Contour plots of the excitation-emission fluorescence matrix for the FCB used for degrading PAHs (a) before and (b) after the catalytic test.

including electron transfer and led to the formation of various radicals. The formed SO₄-• reacted with H₂O and OH-, leading to the formation of HO• (Eqs. 7-8). Therefore, these two radicals might coexist in the FCB/PS system, and SO₄-* consumed by OH-, was replaced by the generated HO• (Liu et al., 2016). Although the generated HO• also had a high reactivity toward PAH, it could also be scavenged by SO₄-• (Eq. 9). Under acidic conditions, Fe²⁺ that was produced from FCB, prompted PS activation with the generation of SO₄-• readily for PAH oxidation (Eq. 10). The conventional mechanism for PS activation was that SO₄-• was generated through one-electron transfer between PS and Fe²⁺ (Eq. 11). Since the enhanced production of O_2^{\bullet} from dissolved oxygen was excluded, it can be deduced that O2- may be mainly generated from the direct decomposition of PS catalyzed by the FCB (Eq. 12) (Wang et al., 2018). From the CV, LSV, and EEFM measurements, it can be inferred that the reversible Fe^{2+}/Fe^{3+} redox equilibrium and π - π interactions between PAH and surface functional groups of CB played the major role on catalytic PAH degradation. The high amorphous carbon content of CB enabled the formation of micropores, which enhanced PAH degradation efficiency, was another reaction mechanism. Therefore, PS activation by FCB led to the generation of abundant SO₄ and HO• favorable PAH degradation. The following reactions briefly described how PS activation by FCB followed by subsequent PAH degradation:

$$S_2O_8^{2-} + 2H_2O \rightarrow HO_2^- + 2SO_4^{2-} + 3H^+$$
 (3)

$$HO_2^- + 2SO_4^{2-} \rightarrow SO_4^{-\bullet} + SO_4^{2-} + H^+ + O_2^{\bullet-}$$
 (4)

$$2S_2O_8^{2-} + 2H_2O \rightarrow 3SO_4^{2-} + SO_4^{\bullet} + 4H^+ + O_7^{\bullet} -$$
 (5)

$$S_2O_8^{2-} + O_2^{\bullet-} \to SO_4^{\bullet-} + SO_4^{2-} + O_2$$
 (6)

$$SO_4^{\bullet\bullet} + H_2O \rightarrow SO_4^{2-} + HO\bullet + H^+$$
 (7)

$$SO_4^{-\bullet} + OH^- \rightarrow SO_4^{2-} + HO\bullet \tag{8}$$

$$SO_4^{-\bullet} + HO_{\bullet} \rightarrow HSO_4^- + 0.5O_2 \tag{9}$$

$$Fe_3O_4 + H^+ \rightarrow \equiv Fe^{2+} + \equiv Fe^{3+} + 4H_2O$$
 (10)

$$\equiv Fe^{2+} + S_2O_8^{2-} \rightarrow \equiv Fe^{3+} + SO_4^{-\bullet} + SO_4^{2-}$$
 (11)

$$\equiv Fe^{3+} + S_2O_8^{2-} + 2H_2O \rightarrow \equiv Fe^{2+} + 2HSO_4^{-} + 2H^{+} + O_2^{\bullet-}$$
 (12)

Fig. 8a shows the production of $SO_4^{\bullet-}$ resulted from the adsorbed PS and immobilized iron on BC surface (Eq. 13 and 14). $SO_4^{\bullet-}$, a major oxidizing agent, reacted with PAHs to produce SO_4^{2-}/OH^- and degradation products (Eq. 15).

$$FCB_{surface}-OOH + S_2O_8^{2-} \rightarrow FCB_{surface}-OO \bullet + SO_4^{-\bullet} + HSO_4-$$
 (13)

$$FCB_{surface} - OH + S_2O_8^{2-} \rightarrow FCB_{surface} - O\bullet + SO_4^{-\bullet} + HSO_4^{-}$$
 (14)

$$SO_4^{-\bullet}/HO_{\bullet} + PAH \rightarrow degradation products + SO_4^{2-}/OH^{-}$$
 (15)

Oxidative ring opening generated small molecular carboxylic acids which were further oxidized to CO_2 and H_2O . The reversible Fe^{2+}/Fe^{3+} couple enabled easy electron transfer for PS activation producing SO_4^{\bullet} . Therefore, the synergistic interaction between Fe^{2+}/Fe^{3+} redox couples and active FCB sites significantly enhanced catalytic activity. Moreover, the standard redox potential of Fe^{2+}/Fe^{3+} is 0.77 V (v.s. NHE), which indicated favorable thermodynamically spontaneous electron transfer from $\equiv Fe^{2+}$ to $\equiv Fe^{3+}$ (Wen et al., 2019).

Based on the literature (Liang et al., 2006; Hadibarata and Kristanti, 2013; Nayebzadeh et al., 2020), a conceptual reaction scheme was established to explain the removal of PAHs from marine sediments by SO₄-• and HO• radicals, produced due to PS activation by FCB. FCB activation of PS produced SO₄-• and HO• and Fe²⁺/Fe³⁺ redox couples enabled efficient electron transfer according to Haber-Weiss mechanism (Dong et al., 2019a). Fig. 8b shows the possible pathway involving reaction between reactive radicals (SO₄−• and HO•) and benzene rings that led to formation of intermediates identified previously by various authors (Liang et al., 2006; Hadibarata and Kristanti, 2013; Navebzadeh et al., 2020). Moreover, hydrogen abstraction, addition on the double bond, and electron transfer were involved in reaction between SO₄[•] and the organic molecules, i.e., intermediates (Matzek and Carter, 2016). According to the proposed degradation pathway, PS activation yielded SO₄-• and HO• which attacked the benzene ring of PAHs and led to the occurrence of a series of hydroxylation, decarboxylation, cleavage of aromatic ring, and formation of intermediates, including 1-hydroxypyrene, cis-4,5-pyrene-dihydrodiol, pyrene-4,5-diol, phenanthrene-4,

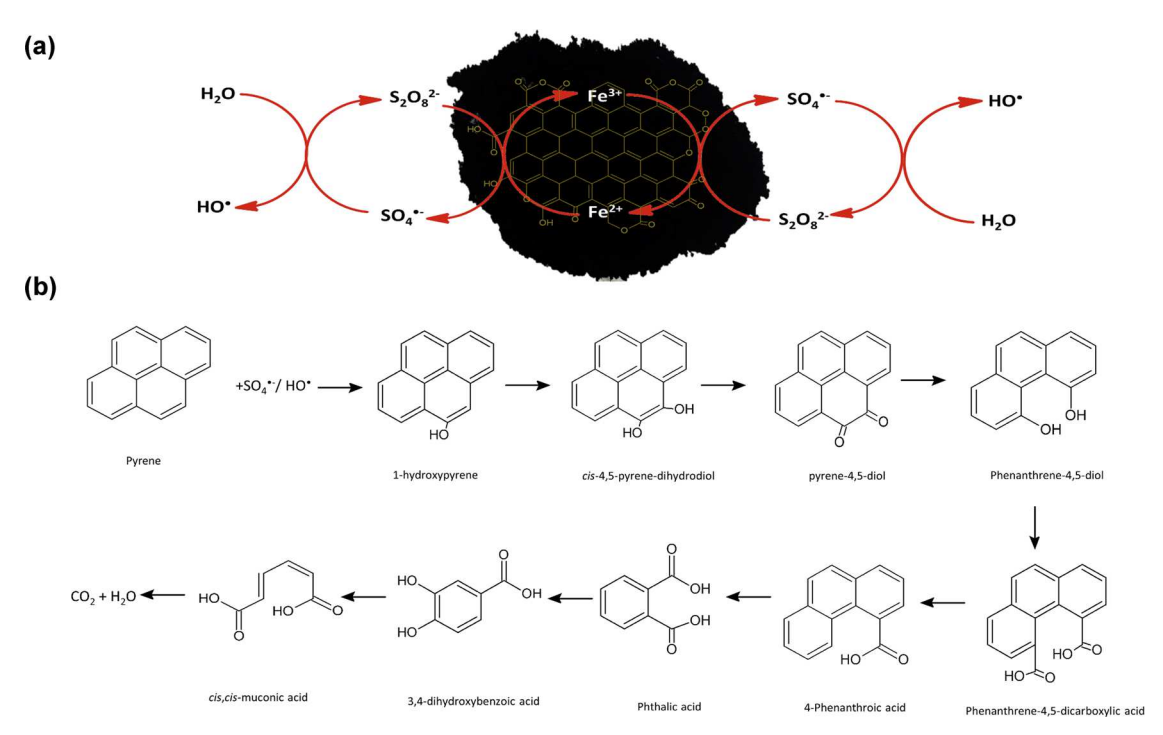


Fig. 8. (a) Proposed degradation mechanism of polycyclic aromatic hydrocarbon (PAH) over FCB catalyst and (b) reaction pathways of pyrene (PY) in the sulfate and hydroxyl radical-based advanced oxidation processes.

5-diol, phenanthrene-4,5-dicarboxylic acid, 4-phenanthroic acid, phthalic acid, 3,4-dihydroxybenzoic acid, and cis,cis-muconic acid. Radical attacks of 1-hydroxypyrene formed cis-4,5-pyrene-dihydrodiol. Moreover, further SO₄-•/HO• attack of *cis*-4,5-pyrene-dihydrodiol at its side chain formed pyrene-4,5-diol. Oxidation and ring opening converted pyrene-4,5-diol to phenanthrene-4,5-diol, phenanthrene-4, 5-dicarboxylic acid, and 4-phenanthroic acid. Further attack on 4-phenanthroic acid by SO₄-•/HO• formed phthalic acid, which was oxidized to 3,4-dihydroxybenzoic acid and cis,cis-muconic acid, which were further mineralized to the small molecular substances carbon dioxide and water. Notwithstanding FCB/PS treatment achieved significant elimination of PAH from contaminated sediments, further studies are necessary to determine the potential side effects of in-situ remediation of PAH-contaminated marine sediments. It is expected that complex matrixes of marine environment will affect the efficiency of the FCB/PS remediation process. Therefore, further studies were necessary to identify reaction byproducts in the treatment of sediments for PAHs removal by PS catalyzed by FCB in order to better understand the degradation mechanism of PAHs. Understanding the nature of reaction intermediates/byproducts is crucial to risk assessment and reduction of PAHs contaminated sediments.

4. Conclusion

The results demonstrated that synergistic interaction between Fe₃O₄ and CB and the activation of persulfate have been applied to remediate the PAHs-contaminated sediment. Surface characterizations showed successful interaction between Fe₃O₄ and CB led to the formation of Fe-O-C bond. Results revealed that the FCB/PS system was promising for the treatment of marine sediments contaminated by PAHs over a broad range of initial pH from 3.0 to 9.0, with increasing ΣPAH removal at acidic pH. At the initial pH of 3.0, the highest ΣPAH degradation was 99, 98%, 97, and 97%, respectively, for the 6-, 5-, 4- and 3-ring PAHs individually. ΣPAH removal reached its plateau as $\Sigma [PAH]$:[PS] ration > $1:10^3$. Langmuir-Hinsheldwood model described the PAH degradation kinetics well. The k_{obs} (1.8 × 10⁻² h⁻¹) at Σ [PAH]: [PS] = 1:10⁴ was almost 2.7 times that of 1:1 ($k_{obs} = 6.6 \times 10^{-3} \text{ h}^{-1}$). The presence of dominant fluorescence components of Fe₃O₄ nanoparticles and CB contributed to the formation of active sites, which might accelerate the degradation of PAHs. The degradation of PAHs followed the pseudofirst-order kinetics model. The degradation rate of PAHs was significantly affected by the initial PS and FCB concentrations, and pH value. FCB was effective in PS activation, which accelerated the production of SO4- and HO radicals for the remediation of PAHs-contaminated marine sediments. FCB-catalyzed PS oxidation will be highly promising and sustainable technique for environmental remediation, i.e., PAHs-contaminated sediments. FCB/PS treatment significantly facilitated the degradation of PAHs in contaminated marine sediments, however, but it must be noted that if applied in-situ, there might be adverse effects on the microbial abundance and community composition of the sediment. As a future perspective, studies on the ecotoxicity of insitu FCB/PS remediation of contaminated sediments are necessary as to ensure that the oxidation products are biodegradable and that the absence of interference by other constituents in the sediments for the safe-by-design of the FCB/PS remediation technology.

CRediT authorship contribution statement

Chang-Mao Hung: Conceptualization, Methodology, Investigation, Validation, Formal analysis, Writing - original draft. Chin-Pao Huang: Writing - review & editing, Visualization. Su Shiung Lam: Writing - review & editing. Chiu-Wen Chen: Resources. Cheng-Di Dong: Resources, Supervision.

Declaration of Competing Interest

The authors declare that they have no known competing financial interests or personal relationships that could have appeared to influence the work reported in this paper.

Acknowledgments

The authors would like to thank the Ministry of Science and Technology of Taiwan, for financial support of this study under Contract Nos. MOST 106-2221-E-022-002-MY3, 106-2221-E-022-003-MY3 and 108-2221-E-992-051-MY3. The authors would like to thank Prof. Wen-Liang Lai from Tajen University for assistance with EEFM measurements and also thank the Dr. Thanh-Binh Nguyen from National Kaohsiung University of Science and Technology for assistance with EPR measurements. The authors would also like to thank Universiti Malaysia Terengganu under Golden Goose Research Grant Scheme (GGRG) (Vot 55191) for supporting Dr. Lam to perform this review project with National Kaohsiung University of Science and Technology. Addition support was provided by US NSF IOA (1632899) to CPH.

Appendix A. Supplementary data

Supplementary material related to this article can be found, in the online version, at doi:https://doi.org/10.1016/j.jece.2020.104440.

References

- M. Ahmad, Q. Yang, Y. Zhang, J. Ling, W. Sajjad, S. Qi, W. Zhou, Y. Zhang, X. Lin, Y. Zhang, J. Dong, The distinct response of phenanthrene enriched bacterial consortia to different PAHs and their degradation potential: a mangrove sediment microcosm study, J. Hazard. Mater. 387 (2019) 120863–120872.
- E. Alveroğlu, H. Sözeri, A. Baykal, U. Kurtan, M. Şenel, Fluorescence and magnetic properties of hydrogels containing Fe₃O₄ nanoparticles, J. Mater. Sci. 1037 (2013) 361–366
- P. Baumard, H. Budzinski, P. Garrigues, J.C. Sorbe, T. Burgeot, J. Belloca, Concentration of PAH in various marine organisms in relation to those in sediments to trophic level, Mar. Pollut. Bull. 36 (1998) 951–960.
- F. Bianco, M. Race, S. Papirio, G. Esposito, Removal of polycyclic aromatic hydrocarbons during anaerobic biostimulation of marine sediments, Sci. Total Environ. 709 (2020) 136141–136151
- I. Bortone, C. Labianca, F. Todaro, S. De Gisi, F. Coulon, M. Notarnicola, Experimental investigations and numerical modelling of in-situ reactive caps for PAH contaminated marine sediments, J. Hazard. Mater. 387 (2020) 121724–121733.
- S. Dimitriadou, Z. Frontistis, A. Petala, G. Bampos, D. Mantzavinos, Carbocatalytic activation of persulfate for the removal of drug diclofenac from aqueous matrices, Catal. Today (2020), https://doi.org/10.1016/j.cattod.2019.02.025.
- C.D. Dong, C.W. Chen, C.M. Hung, Synthesis of magnetic biochar from bamboo biomass to activate persulfate for the removal of polycyclic aromatic hydrocarbons in marine sediments, Bioresour. Technol. 245 (2017a) 188–195.
- C.D. Dong, C.W. Chen, C.M. Hung, Preparing carbon–black–coated magnetite nanoparticles: Fabrication, characterization, and heterogeneous persulfate oxidation of methylene blue, Desalination Water Treat. 63 (2017b) 357–365.
- C.D. Dong, C.W. Chen, C.M. Kao, C.C. Chien, C.M. Hung, Wood-biochar-supported magnetite nanoparticles for remediation of PAH-contaminated estuary sediment, Catalysts 8 (2018a) 73–86.
- C.D. Dong, M.L. Tsai, C.W. Chen, C.M. Hung, Remediation and cytotoxicity study of polycyclic aromatic hydrocarbon-contaminated marine sediments using synthesized iron oxide–carbon composite, Environ. Sci. Pollut. Res. 6 (2018b) 5243–5253.
- C.D. Dong, Y.C. Lu, J.H. Chang, T.H. Wang, C.W. Chen, C.M. Hung, Enhanced persulfate degradation of PAH-contaminated sediments using magnetic carbon microspheres as the catalyst substrate, Process Safety Environ. Protect. 125 (2019a) 219–227.
- C.D. Dong, C.W. Chen, M.L. Tsai, C.M. Hung, The efficacy and cytotoxicity of iron oxide-carbon black composites for liquid-phase toluene oxidation by persulfate, Environ. Sci. Pollut. Res. 26 (2019b) 14786–14796.
- C.D. Dong, C.W. Chen, M.L. Tsai, J.H. Chang, S.Y. Lyu, C.M. Hung, Degradation of 4nonylphenol in marine sediments by persulfate over magnetically modified biochars, Bioresour, Technol. 281 (2019c) 143–148.
- C.D. Dong, C.P. Huang, T.B. Nguyen, C.F. Hsiung, C.H. Wu, Y.L. Lin, C.W. Chen, C. M. Hung, The degradation of phthalate esters in marine sediments by persulfate over iron–cerium oxide catalyst, Sci. Total Environ. 696 (2019d) 133973–133982.
- C.D. Dong, C.W. Chen, M.L. Tsai, C.M. Hung, The efficacy and cytotoxicity of iron oxidecarbon black composites for liquid-phase toluene oxidation by persulfate, Environ. Sci. Pollut. Res. 26 (2019e) 14786–14796.
- C.D. Dong, M.L. Tsai, T.H. Wang, J.H. Chang, C.W. Chen, C.M. Hung, Removal of polycyclic aromatic hydrocarbon (PAH)-contaminated sediments by persulfate oxidation and determination of degradation product cytotoxicity based on HepG2

- and ZF4 cell lines, Environ. Sci. Pollut. Res. (2020a), https://doi.org/10.1007/s11356-019-04421-w.
- C.D. Dong, C.W. Chen, T.B. Nguyen, C.P. Huang, C.M. Hung, Degradation of phthalate esters in marine sediments by persulfate over Fe–Ce/biochar composites, Chem. Eng. J. 384 (2020b), 123301.
- J. Du, C. Jing, Anthropogenic PAHs in lake sediments: A literature review (2002–2018), Environ. Sci. Proc. Impacts 20 (2018) 1649–1666.
- E. Ferrarese, G. Andreottola, I.A. Oprea, Remediation of PAH-contaminated sediments by chemical oxidation, J. Hazard. Mater. 152 (2008) 128–139.
- F. Ghanbari, M. Moradi, Application of peroxymonosulfate and its activation methods for degradation of environmental organic pollutants: Review, Chem. Eng. J. 310 (2017) 41_62
- L. Giovanni, M. Diego, L. Giusy, G. Marco, C. Marco, A. Francesco, C. Barbara, N. Michele, Toxicity assessment within the application of in situ contaminated sediment remediation technologies: A review, Sci. Total Environ. 621 (2018) 85–94.
- T. Hadibarata, R.A. Kristanti, Biodegradation and metabolite transformation of pyrene by basidiomycetes fungal isolate Armillaria sp. F022, Bioprocess Biosyst. Eng. 36 (2013) 461–468.
- B. Han, L. Zheng, F. Lin, Risk assessment and source apportionment of PAHs in surface sediments from Caofeidian Long Island, China, Mar. Pollut. Bull. 145 (2019) 42–46.
- C.M. Hung, C.W. Chen, Y.Y. Liu, C.D. Dong, Decolorization of methylene blue by persulfate activated with FeO magnetic particles, Water Envir. Res. 88 (2016a) 675–686.
- C.M. Hung, C.W. Chen, Y.J. Jhuang, C.D. Dong, Fe₃O₄ magnetic nanoparticles: Characterization and performance exemplified by the degradation of methylene blue in the presence of persulfate, J. Adv. Oxid. Technol. 19 (2016b) 43–51.
- C.M. Hung, C.P. Huang, S.L. Hsieh, M.L. Tsai, C.W. Chen, C.D. Dong, Biochar derived from red algae for efficient remediation of 4-nonylphenol from marine sediments, Chemosphere 254 (2020a), 126919.
- C.M. Hung, C.P. Huang, S.K. Chen, C.W. Chen, C.D. Dong, Electrochemical analysis of naproxen in water using poly(L-serine)-modified glassy carbon electrode, Chemosphere 254 (2020b), 126686.
- S. Kamari, A. Shahbazi, Biocompatible Fe₃O₄@SiO₂-NH₂ nanocomposite as a green nanofiller embedded in PES-nanofiltration membrane matrix for salts, heavy metal ion and dye removal: Long-term operation and reusability tests, Chemosphere 243 (2020) 125282-125293.
- M. Kołtowski, I. Hilber, T.D. Bucheli, B. Charmas, J. Skubiszewska-Zięba, P. Oleszczuk, Activated biochars reduce the exposure of polycyclic aromatic hydrocarbons in industrially contaminated soils, Chem. Eng. J. 310 (2020) 33–40.
- A. Kumar, M. Khan, L. Fang, I.M.C. Lo, Visible-light-driven N-TiO₂@SiO₂@Fe₃O₄ magnetic nanophotocatalysts: Synthesis, characterization, and photocatalytic degradation of PPCPs, J. Hazard. Mater. 370 (2019) 108–116.
- L. Li, C. Lai, F. Huang, M. Cheng, G. Zeng, D. Huang, B. Li, S. Liu, M. Zhang, L. Qin, M. Li, J. He, Y. Zhang, L. Chen, Degradation of naphthalene with magnetic bio-char activate hydrogen peroxide: Synergism of bio-char and FeMn binary oxides, Water Res. 160 (2019) 238–248.
- Y. Liang, D.R. Gardner, C.D. Miller, D. Chen, A.J. Anderson, B.C. Weimer, R.C. Sims, Study of biochemical pathways and enzymes involved in pyrene degradation by Mycobacterium sp. strain KMS, Appl. Environ. Microbiol. 72 (2006) 7821–7828.
- Y. Liu, X. He, Y. Fu, D.D. Dionysiou, Kinetics and mechanism investigation on the destruction ofoxytetracycline by UV-254 nm activation of persulfate, J. Hazard. Mater. 305 (2016) 229–239.
- Z. Liu, X. Li, Z. Rao, F. Hu, Treatment of landfill leachate biochemical effluent using the nano-Fe₃O₄/Na₂S₂O₈ system: Oxidation performance, wastewater spectral analysis, and activator characterization, J. Environ. Manage. 208 (2018) 159–168.
- J. Liu, J. Jiang, Y. Meng, A. Aihemaiti, Y. Xu, H. Xiang, Y. Gao, X. Chen, Preparation, environmental application and prospect of biochar-supported metal nanoparticles: A review, J. Hazard. Mater. 388 (2020), 122026.
- X. Lu, D. Wang, K.H. Wu, X. Guo, W. Qi, Oxygen reduction to hydrogen peroxide on oxidized nanocarbon: Identification and quantification of active sites, J. Colloid Interface Sci. 573 (2020) 376–383.
- S.P. Maletić, J.M. Beljin, S.D. Rončević, M.G. Grgić, B.D. Dalmacija, State of the art and future challenges for polycyclic aromatic hydrocarbons is sediments: sources, fate, bioavailability and remediation techniques, J. Hazard. Mater. 365 (2019) 467–482.
- L.W. Matzek, K.E. Carter, Activated persulfate for organic chemical degradation: A review, Chemosphere. 151 (2016) 178–188.
- Y. Meng, X. Liu, S. Lu, T. Zhang, B. Jin, Q. Wang, Z. Tang, Y. Liu, X. Guo, J. Zhou, B. Xi, A review on occurrence and risk of polycyclic aromatic hydrocarbons (PAHs) in lakes of China, Sci. Total Environ. 651 (2019) 2497–2506.

- D. Merhaby, S. Rabodonirina, S. Net, B. Ouddane, J. Halwani, Overview of sediments pollution by PAHs and PCBs in mediterranean basin: Transport, fate, occurrence, and distribution, Mar. Environ. Res. 149 (2019) 110646–110660.
- M. Nayebzadeh, M. Vahedpour, A. Shiroudi, J.M. Rius-Bartra, Kinetics and oxidation mechanism of pyrene initiated by hydroxyl radical. A theoretical investigation, Chem. Phys. 528 (2020) 110522–110668.
- J.F. Ontiveros-Cuadras, A.C. Ruiz-Fernández, J.A. Sanchez-Cabeza, J. Sericano, L. H. Pérez-Bernal, F. Páez-Osuna, R.B. Dunbar, D.A. Mucciarone, Recent history of persistent organic pollutants (PAHs, PCBs, PBDEs) in sediments from a large tropical lake, J. Hazard. Mater. 368 (2019) 264–273.
- O.P. Siwach, P. Sen, Fluorescence properties of Fe nanoparticles prepared by electroexplosion of wires, Mater. Sci. Eng. B 149 (2008) 99–104.
- Z. Pi, X. Li, D. Wang, Q. Xu, Z. Tao, X. Huang, F. Yao, Y. Wu, L. He, Q. Yang, Persulfate activation by oxidation biochar supported magnetite particles for tetracycline removal: Performance and degradation pathway, J. Clean. Prod. 235 (2019) 1103–1115.
- M. Peluffo, F. Pardo, A. Santos, A. Romero, Use of different kinds of persulfate activation with iron for the remediation of a PAH-contaminated soil, Sci. Total Environ. 563–564 (2016) 649–656.
- C. Qin, H. Wang, X. Yuan, T. Xiong, J. Zhang, J. Zhang, Understanding structure-performance correlation of biochar materials in environmental remediation and electrochemical devices, Chem. Eng. J. 382 (2020) 122977–122999.
- A.U. Rajapaksha, Y.S. Ok, A. El-Naggar, H. Kim, F. Song, S. Kang, Y.F. Tsang, Dissolved organic matter characterization of biochars produced from different feedstock materials, J. Environ. Manage. 233 (2019) 393–399.
- L. Ren, H. Lin, F. Meng, F. Zhang, One-step solvothermal synthesis of Fe₃O₄@Carbon composites and their application in removing of Cr (VI) and Congo red, Ceram. Int. 45 (2019) 9646–9652.
- W. Song, P. Ge, Q. Ke, Y. Sun, F. Chen, H. Wang, Y. Shi, X. Wu, H. Lin, J. Chen, C. Shen, Insight into the mechanisms for hexavalent chromium reduction and sulfisoxazole degradation catalyzed by graphitic carbon nitride: The Yin and Yang in the photoassisted processes, Chemosphere 221 (2019) 166–174.
- C. Sun, T. Chen, Q. Huang, M. Zhan, X. Li, J. Yan, Activation of persulfate by CO2-activated biochar for improved phenolic pollutant degradation: Performance and mechanism, Chem. Eng. J. 380 (2020), 122519.
- H.B. Truong, J.A. Ike, Y.S. Ok, J. Hur, Polyethyleneimine modification of activated fly ash and biochar for enhanced removal of natural organic matter from water via adsorption, Chemosphere 243 (2020) 125454–125462.
- Q. Wang, B. Wang, Y. Ma, S. Xing, Enhanced superoxide radical production for ofloxacin removal via persulfate activation with Cu-Fe oxide, Chem. Eng. J. 354 (2018) 473–480.
- Z. Wang, Y. Chen, L. Chen, S. Xi, Y. Liu, Y. Dong, L. Miao, Ex-situ treatment of sediment from a black-odor water body using activated sludge, Sci. Total Environ. 713 (2020), 136651.
- X. Wu, G. Xu, J. Zhu, Sonochemical synthesis of Fe₃O₄/carbon nanotubes using low frequency ultrasonic devices and their performance for heterogeneous sonopersulfate process on inactivation of *Microcystis aeruginosa*, Ultrason. Sonochem. 58 (2019) 104634–104641
- C. Yang, Y. Liu, X. Sun, S. Miao, Y. Guo, T. Li, Characterization of fluorescent dissolved organic matter from green macroalgae (*Ulva prolifera*)-derived biochar by excitationemission matrix combined with parallel factor and self-organizing maps analyses, Bioresour, Technol. 287 (2019a) 121471–121475.
- X. Yang, A. Tsibart, H. Nam, J. Hur, A. El-Naggar, F.M.G. Tack, C.H. Wang, Y.H. Lee, D.C. W. Tsang, Y.S. Ok, Effect of gasification biochar application on soil quality: Trace metal behavior, microbial community, and soil dissolved organic matter, J. Hazard. Mater. 365 (2019b) 684–694.
- F. Yin, C. Wang, K.Y.A. Lin, S. Tong, Persulfate activation for efficient degradation of norfloxacin by a rGO-Fe₃O₄ composite, J. Taiwan Inst. Chem. Eng. 102 (2019) 163–169.
- M. Zhang, Y. Feng, K. Zhang, Y. Wang, X. Pan, Impact of salinity on colloidal ozone aphrons in removing phenanthrene from sediments, Chem. Eng. J. 384 (2020a), 121436.
- L. Zhang, B. Liu, J. Li, A novel synthesis method of mesoporous carbon loaded with Fe₃O₄ composite for effective adsorption and degradation of sulfamethazine, J. Mol. Liq. 299 (2020b) 112096–112108.
- L. Zhu, L. Meng, J. Shi, J. Li, X. Zhang, M. Feng, Metal-organic frameworks/carbon-based materials for environmental remediation: A state-of-the-art mini-review, J. Environ. Manage. 232 (2019) 964–9778.

Support Information

The remediation of marine sediments contaminated by polycyclic aromatic hydrocarbons (PAHs) using persulfate over a nano-sized iron composite of magnetite and carbon black activator

Chang-Mao Hung^a, Chin-Pao Huang^b, Su Shiung Lam^c, Chiu-Wen Chen^a, Cheng-Di Dong^{a,*}

^a Department of Marine Environmental Engineering, National Kaohsiung University of Science and Technology, Kaohsiung City, Taiwan.

^b Department of Civil and Environmental Engineering, University of Delaware, Newark, USA.

^c Pyrolysis Technology Research Group, Institute of Tropical Aquaculture and Fisheries (Akuatrop) & Institute of Tropical Biodiversity and Sustainable Development (Bio-D Tropika), Universiti Malaysia Terengganu, 21030, Kuala Terengganu, Terengganu, Malaysia.

S1. Characterization of FCB

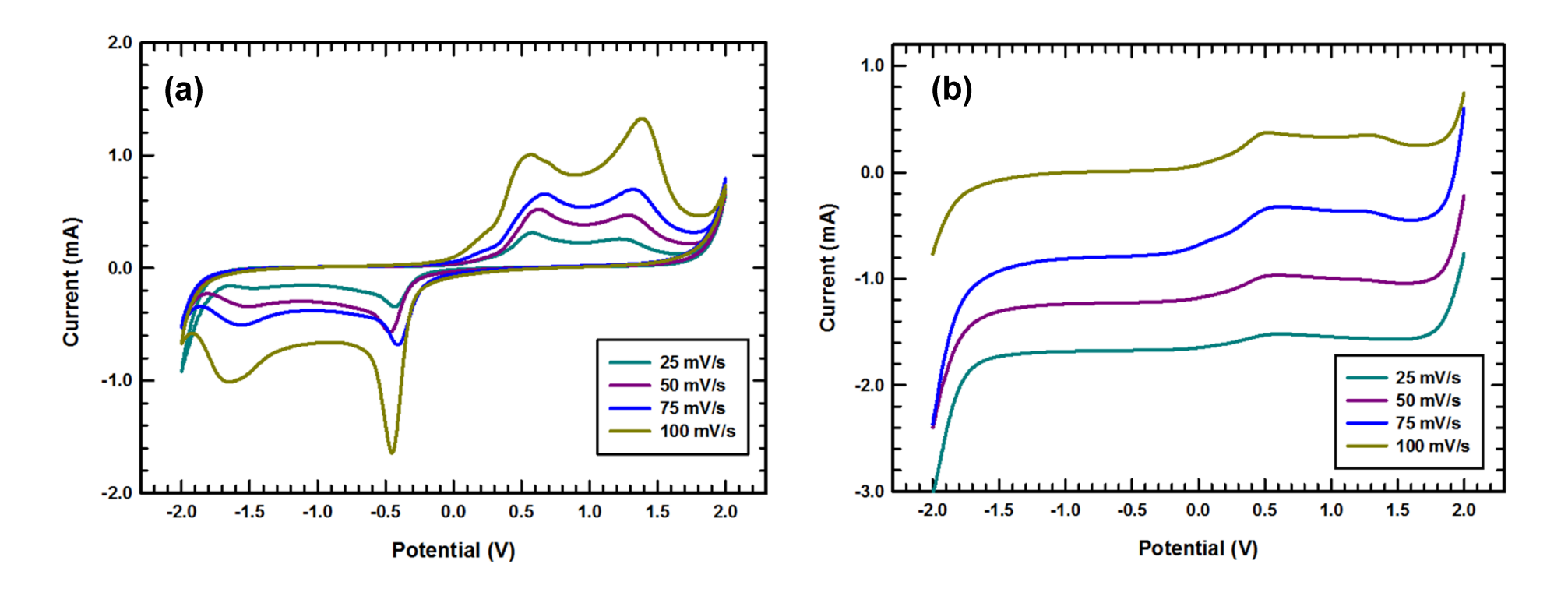


Fig. S1. (a) Cyclic voltammogram (CV) and (b) linear sweep voltammetry (LSV) for the FCB catalyst at different scan rates ranging from 25 to 100 mV/s in 0.5 M Na2SO4 solution.

S2. Characterization of sediments

Table S1 Physico-chemical composition of the raw sediment. Values expressed in dry weight.

Characteristics	Value
Clay (< 2 μm, %)	5.0
Silt (2–63 μm, %)	61.0
Sand (> 63 μm, %)	34.0
Water content (%)	83.1
рН	6.7
Total organic carbon (TOC, %)	6.4
Total nitrogen (TN, mg/kg)	1540
Total phosphorus (TP, mg/kg)	537

S3. Derivation of kinetics equation

According to the Langmuir-Hinshelwood kinetics of heterogeneous catalysis, adsorption of reactants onto the catalyst surface is the first reaction step. Assuming that at the onset of the reaction, SPS adsorbs onto the active site, S_A , and PAH adsorbs onto the different active site, S_B , of the FCB composite, rapidly, according to the following equilibrium reactions:

$$S_A + PS \rightleftharpoons S_A - PS; K_1$$
 (S1)

$$S_B + PAH \Rightarrow S_B - PAH; K_2$$
 (S2)

where K_1 and K_2 are the adsorption equilibrium constants of PS and PAH on the different active sites of FCB, respectively. S_A -PS and S_B -PAH are the adsorbed PS and PAH species on the FCB surface, respectively. The reaction between the adsorbed PS and PAH is the rate-limiting step, that is,

$$S_A$$
-PS + S_B -PAH \rightarrow products + S_A + S_B ; k_3 (rate-limiting step) (S3)

From Eq. (3), one has the rate expression:

$$rate(r) = -\frac{d[PAH]}{dt} = k_3 [S_A - PS][S_B - PAH]$$
 (S4)

where k_3 is the reaction rate constant. From Eq. S1 and Eq. S2, one has:

$$[S_A-PS] = K_1[S_A][PS]$$
(S5)

and

$$[S_B-PAH] = K_2[S_B][PAH]$$
 (S6)

From the following mass balance relationship, one has:

$$S_A^T = [S_A] + [S_A - PS]$$
(S7)

and

$$S_B^T = [S_B] + [S_B - PAH]$$
 (S8)

Combing Eq. S5 and Eq. S7 and Eq.S6 and Eq.S8, one has:

$$[S_A - PS] = \frac{S_A^T K_1[PS]}{1 + K_1[PS]}$$
 (S9)

and

$$[S_B - PAH] = \frac{S_B^T K_2[PAH]}{1 + K_2[PAH]}$$
 (S10)

By substituting Eq. S9 and Eq. S10 into Eq. S4, the reaction rate expression is:

$$r = -\frac{a[PAH]}{at} = k_3 \times \frac{S_A^T K_1[PS]}{1 + K_1[PS]} \times \frac{S_B^T K_2[PAH]}{1 + K_2[PAH]}$$
(S11)

If $1 \gg K_1[PS]$ and $1 \gg K_2[PAH]$, Eq. S11 becomes:

$$r = k_3 S_A^T K_1[PS] S_B^T K_2[PAH] = k_{app}[PS][PAH]$$
 (S12)

Where $k_{app} = k_3 S_A^T K_1[PS] S_B^T K_2$. At a constant PS concentration and [PS] >> [PAH],

the catalytic oxidation of PAH follows the following first-order kinetics:

$$\mathbf{r} = k_{obs}[PAH] \tag{S13}$$

where
$$k_{obs} = k_{app}[PS]$$
 (S14)

Eq. (S14) predicts a first-order kinetics for the degradation of PAH.

Note that k_{obs} is a function of the product of S_A and S_B . By expressing both sites as a function of total surface site, S_T , as α_A and α_B , and that $\alpha_A + \alpha_B = 1$, one has

$$k_{\text{obs}} \propto S_T^2 \alpha_A \alpha_B = S_T^2 (1 - \alpha_A) \alpha_A$$
 (S15)

Eq. (S15) predicts k_{obs} as a function of FCB dosage with a peak k_{obs} around $\alpha_A = \alpha_B =$

0.5. Therefore it is expected that the rate constant will be at the maximum when the surface site for the specific adsorption of PS and PAHs are equal.